International Journal of Thermal Sciences 206 (2024) 109340

Contents lists available at ScienceDirect

International Journal of Thermal Sciences

journal homepage: www.elsevier.com/locate/ijts

Nucleate pool boiling bubble dynamics for R32 and R1234yf on machined micro-structured surfaces

W.J. van den Bergh [a,**], M. Whiting [a], P.E. Theodorakis [b], M. Everts [a,c,*]

[a] University of Pretoria, Lynnwood, 0028 Pretoria, South Africa
[b] Institute of Physics, Polish Academy of Sciences, Al. Lotników 32/46, 02-668 Warsaw, Poland
[c] University College London, London, WC1E 7JE, United Kingdom

ARTICLE INFO

Keywords:
Nucleate boiling
Bubble dynamics
Numerical
Engineered surfaces

ABSTRACT

Efficient electronics cooling has always been a perpetual challenge, with the limits of single-phase cooling almost being reached. Two-phase cooling in the form of pool boiling is an attractive next step, with much research being devoted to it. While refrigerants operating at lower saturation temperatures are key to achieving effective cooling, surface modifications have been shown to also affect bubble dynamics and enhance nucleate pool boiling heat transfer. A simple, easy to implement fabrication method was sought, with the goal of expanding the knowledge of bubble dynamics. To this end, single bubble growth on structured surfaces that are achievable on a lathe, with an average roughness of 75 μm and differing indentation angles between 90° and 46°, was studied numerically using an OpenFOAM multiphase library. Conjugate heat transfer was applied, with heat fluxes ranging between 7.6 and 28 kW/m^2 for pure refrigerants R32 and R1234yf. By comparing the bubble equivalent diameter with that of a smooth surface at a fixed heat flux, it was found that the bubble growth rates of structured surfaces were largely independent of indentation angles less than 90°, but lower than for smooth surfaces. For structured surfaces, a critical indentation angle of approximately 60° was identified which affected the bubble dynamics. For angles greater than the critical angle the bubble growth time was up to 150 % longer, which also resulted in larger departure diameters. However, the opposite trend was observed as the indentation angle was decreased below the critical angle. From a force analysis, it was found that the physical limitation imposed on the bubble growth was responsible for the critical indentation angle behaviour, with the most acute angle of 46° showing the shortest departure time. Furthermore, the bubble growth from a single cavity corresponded better with the trends of a smooth surface than a structured surface with comparable indentation angles. On a structured surface, once the bubble reached the edge of the cavity, its base diameter was limited by the physical characteristics of the surface. For the single cavity surface, however, bubble growth was uninhibited beyond the cavity, mimicking a completely smooth surface. The marked difference between results of a fully structured surface and the single cavity implies that future research will have to take the structural limitations on bubble growth imposed by a roughened surface into account.

1. Introduction

With the continual increase in computational power, the need for CPU cooling has become an ever more active field of research in the last few years. Single-phase forced convection cooling is reaching its limits, and the next step is to implement two-phase cooling. To this end, immersion cooling coupled with nucleate boiling is a promising two-phase cooling method, but it comes with a series of challenges, akin to the initial development of free convection air-cooled heat sinks. As the boiling process is strongly dependent on the heat transfer surface and fluid used, it is important to obtain a surface that will provide a steady, predictable means of removing heat, while also keeping costs and manufacturability in mind.

Purified, demineralised water is one of the obvious choices for immersion cooling, but the high boiling temperature and conductivity of water at atmospheric temperature make it unsuitable for electronics cooling, introducing some additional complications in maintaining sub-atmospheric pressures. Instead, low temperature, low pressure refrigerants are a promising alternative that have been the topic of much

* Corresponding author. University College London, London, WC1E 7JE, United Kingdom.
** Corresponding author.
E-mail addresses: wj.vandenbergh@up.ac.za (W.J. van den Bergh), m.everts@ucl.ac.uk (M. Everts).

https://doi.org/10.1016/j.ijthermalsci.2024.109340
Received 7 December 2023; Received in revised form 15 July 2024; Accepted 13 August 2024
Available online 17 August 2024

Nomenclature

Co	Courant number [−]
c	Specific heat [J/kg°C]
D	Diameter [m]
F	Force [N]
g	Gravitational acceleration [m/s^2]
h	Enthalpy [J/kg]
P	Pressure [Pa]
R	Roughness [m]
q	Heat flux [W/m^2]
t	Time [s]
T	Temperature [°C]
V	Volume [m^3]

Superscripts

*	Normalised
i	Placeholder for either liquid or vapour
l	Liquid
v	Vapour

Subscripts

a	Average
B	Buoyancy
base	Base of bubble
bub	Bubble
eq	Equivalent
int	Interface
KC	Kays and Crawford
net	Net
p	Isobaric
pc	Phase change
rgh	Pressure without hydrostatic contribution
s	Solid
S	Surface tension
sat	Saturation
w	Wall

Greek letters

α	Phase fraction [−]/Thermal diffusivity [m^2/s]/ Indentation angle [°]
β	Thermal expansion coefficient [1/°C]/Vertical angle [°]
δ	Dirac delta [−]/Thickness [m]
λ	Thermal conductivity [W/m°C]
ρ	Density [kg/m^3]
μ	Dynamic viscosity [Pa.s]
θ	Contact angle [°]
σ	Surface tension [N/m]

research, although the global warming potential of these refrigerants remain a concern. Regardless of which fluid is used, the study of bubble dynamics remains of prime importance as a thorough understanding of the boiling process assists in optimising the cooling method.

With the intense research attention dedicated to this field, many studies have been published. According to an account by Mohanty and Das [1], bubble departure size and frequency as well as active nucleation site density are major contributors to nucleate boiling heat transfer. Of note is that the surface roughness seemed to be insignificant in the development of bubble growth or departure correlations. Many studies investigated bubble dynamics from smooth and rough surfaces, both on plates and tubes [2–5].

Moreover, regarding the surface roughness of horizontal plates, relevant experimental research by McHale and Garimella [2] on the pool boiling of FC-77 indicated that the bubble departure diameter decreases and bubble departure frequency increases for roughened surfaces in comparison with smooth substrates. In their study, the rough surface had an average roughness of 5.89 μm and was compared to a nominally smooth surface with an average roughness of 0.03 μm. Active nucleation site density increased with both wall superheat and roughness. In a similar study on the experimental pool boiling of PF-5060, Suszko and El-Genk [3] also found that the bubble departure diameter was lower and the departure frequency was higher for roughened surfaces with an average roughness from 0.21 to 1.79 μm compared to the nominally smooth surface with a roughness of 0.0039 μm. Nucleation site density increased with roughness, while the departure diameter and frequency were found to be largely independent of the level of roughness considered.

In general, three strategies are followed to modify bubble behaviour [6]: (1) fluid modification, (2) passive surface modification, and (3) active external fields. Passive surface modification, which is the focus of this study, includes porous coatings, modification of wettability, and the introduction of micro- and nano-structures. While nano- and micro-coatings on surfaces offer a very attractive way of modifying bubble dynamics and increasing nucleate boiling effectiveness, the fabrication cost and fragility of many of the proposed methods [7,8] raises questions on the practicality of such methods.

Nucleate boiling of water on a composite surface of macro- and micropores and dendritic structures obtained by electrochemical methods was studied experimentally by Xu et al. [9]. The macropores were on the scale of approximately 200 μm, the micropores 2 μm, and the dendritic structures 0.4 μm. They found that this combination improved both the heat transfer coefficients and critical heat fluxes at heat fluxes below 100 kW/m^2 and above 600 kW/m^2. The micro- and nano-structures increased nucleation site density, with the macropores influencing bubble size and departure rates. Under high heat fluxes exceeding 400 kW/m^2, the bubbles were not only larger, but also grew approximately three times faster than from a smooth surface.

Li et al. [10] leveraged alternating hydrophobic and hydrophilic surfaces in a carefully constructed grid in an attempt to fine-tune experimental bubble behaviour. This was achieved by coating a smooth polished copper surface in a hydrophobic film, then sintering hydrophilic copper wires of diameters 20–50 μm in a mesh on top of the film. A numerical study to complement the experimental work was also performed, without taking conjugation into account. It was found that the hybrid surface offered an adaptable way of tuning bubble behaviour by altering the ratio of hydrophilic to hydrophobic surfaces.

Focusing on structured surfaces, Wang et al. [11] performed a numerical study of the effect of structured hemispherical indentations and protrusions with a radius of 1 mm on the heat transfer and critical heat flux of boiling water at atmospheric conditions. It was found that the surface modifications both exhibited a decreased superheat for the same heat flux compared to a smooth surface. The indentations provided the best heat transfer at the cost of a lower critical heat flux.

Song et al. [12] experimentally demonstrated a simple technique for enhancement in both heat transfer coefficient and critical heat flux of boiling water by using sandblasted silicon surfaces. The arithmetic mean roughness-value of these surfaces depended on the particle size used during the sandblasting. The roughness ranged from 0.5 to 8 μm, corresponding to particle sizes ranging from 25 to 150 μm. The results showed a significant increase in heat transfer coefficient of 433 % and in critical heat flux of 193 % over smooth silicon for the coarsest abrasive surface.

Another simple manufacturing technique for structured surfaces was

employed by Nirgude et al. [13] utilising electric discharge machining. Structured surfaces were fabricated with what amounts to square pin fins on the boundary between macro- and microscale. The structures were chosen to explore two different heights of 1000 and 500 μm respectively, with a width of 900 μm and differing gaps between fins of 725 and 610 μm. It was found that any structured geometry provided better heat transfer performance than a smooth surface for both the water and isopropyl alcohol they considered. It was also common to see a lesser wall superheat at boiling initialisation for the structured surfaces, and that the depth of the structures had a definite impact on the heat transfer enhancement for water while not being significant for isopropyl alcohol.

According to Honda and Wei [14], microscale pin fins were most effective at increasing the critical heat flux, while surface roughness achieved by, for example, sandblasting, was effective but no direct link between the roughness parameter and the thermal enhancement existed. They also found that microstructures act to increase the bubble departure time. In an experimental study on boiling FC-72 by Wei and Honda [15], microscale pin fins of heights between 60 and 270 μm and thickness of 30 and 50 μm, directly dry etched onto silicon computer chips were evaluated. They found a considerable increase in heat transfer and critical heat flux as compared to a smooth chip, with fins of height 270 μm and thickness 50 μm showing the greatest improvement in critical heat flux.

On the one hand, while nucleate boiling processes can be significantly improved with carefully controlled surface enhancement processes [9,10], these processes might not necessarily suitable to be implemented on an industrial scale due to a combination of fragility, expense, and manufacturing difficulty. On the other hand, simple surface modifications such as fins and pins on a microscale level of between 50 and 1000 μm show much promise [11,13,15]. However, experimental work, even for these simple surfaces, is fraught with difficulty and expense.

Taking advantage of the simplicity of numerical versus experimental work with regards to investigating a wide range of different surfaces, the focus of this study was to investigate engineered surfaces with an emphasis on ease of manufacture. Different topologies were created by imposing different indentation angles, achievable on a lathe, with a fixed average roughness of 75 μm over an entire surface. R32 and R1234yf, two refrigerants that are being considered for use in CPU cooling, were evaluated. The engineered surfaces were compared to a smooth surface as well as to a single cavity to determine the effect of conjugate heat transfer and the extended surface topology on bubble dynamics. This provided valuable insight into the boiling characteristics of machined surfaces that could feasibly be found in industry.

2. Numerical model

Numerical simulations were performed using the OpenFOAM framework, coupled with an open-source multiphase boiling library, *TwoPhaseFlow* [16]. This library included three different OpenFOAM solvers, each building on the previous and increasing in complexity. Coupled with extensible, modular models for phase change and surface tension, and validated analytically, the code provided a solid foundation for simulation of heat and mass transfer across a fluid interface. The governing equations and assumptions for the computational fluid dynamics model are briefly discussed in this paper, with the full detail of the equations available in Scheufler and Roenby [16].

The microlayer contribution to the heat transfer and bubble growth was neglected in this study. This decision was made after observing that it did not play a major role for pure refrigerants in the experimental and numerical studies of Li et al. [17,18], which were used to validate the results obtained in this study. Li et al. [17,18] found that the bubble growth was predicted remarkably well by the correlation of Sakashita [19], and that the microlayer appeared to evaporate in approximately 25 ms for pure R32. This is in good agreement with Kim [20] who asserted that a large part of observed bubble growth was due to the heat gained at the bubble cap which is largely independent of the processes at the wall. As the microlayer of the fluid between the bubble and the surface accounted for at most approximately 25 % of the heat transfer in the first few microseconds of bubble growth, it can be ignored.

2.1. Governing equations

The multiRegionPhaseChangeFlow solver in *TwoPhaseFlow* was used. This is a compressible, non-isothermal solver that accounts for phase change and conjugate heat transfer, using a Volume of Fluid method for interface tracking. The assumption was made that the flow was incompressible, leading to the following phase continuity equation:

$$\frac{\partial \alpha}{\partial t} + \nabla \bullet (\boldsymbol{u}\alpha) = \dot{\alpha}_{pc} \tag{1}$$

where α is the volume fraction, $\boldsymbol{u}$ is the velocity field, and α_{pc} is the explicit source term accounting for phase change.

With the added assumption of laminar flow, the Navier-Stokes equation reduced to:

$$\frac{\partial(\rho \boldsymbol{u})}{\partial t} + \nabla(\rho \boldsymbol{u}\boldsymbol{u}) - \nabla \cdot \left\{\mu\left(\nabla \boldsymbol{u} + (\nabla \boldsymbol{u})^T\right)\right\} = -\nabla p_{rgh} + (\boldsymbol{g} \cdot \boldsymbol{x})(\rho_l - \rho_v)\hat{\boldsymbol{n}}_{int}\delta_{int} + \boldsymbol{f} \tag{2}$$

where μ is the dynamic viscosity, $\boldsymbol{g}$ and $\boldsymbol{x}$ the gravity and position vector, respectively, $\hat{\boldsymbol{n}}_{int}$ a unit normal vector on the interface surface pointing into the denser fluid, and δ_{int} the Dirac delta function at this interface. Additional source terms, such as surface tension, were taken into account with the term $\boldsymbol{f}$. In the interest of numerical efficiency, the pressure term was replaced by the auxiliary term p_{rgh}, defined as:

$$p_{rgh} = p - (\boldsymbol{g} \cdot \boldsymbol{x})\rho \tag{3}$$

This represents the pressure, p, with the hydrostatic component removed and has the advantage of the Dirac delta function only being non-zero at the interface between the liquid and vapour. It should be noted that quantities that were averaged in a finite volume framework contained contributions of both liquid and vapour at the interface.

The energy equation for the fluid is given as:

$$\frac{\partial \alpha^i \rho^i c_p^i T^i}{\partial t} + \nabla \cdot \left(\alpha^i \rho^i c_p^i T^i \boldsymbol{u}\right) = \nabla \cdot \left(\lambda^i \nabla T^i\right) + \dot{q}_{pc}^i \tag{4}$$

Since the two-field approach was adopted, the superscript i can either be v for vapour or l for liquid. The energy change due to phase change is denoted by the source term $\dot{q}_{pc}^i$. Conjugate heating was accounted for using the following heat transfer equation:

$$\frac{\partial \rho^s h^s}{\partial t} - \nabla \cdot \left(\frac{\lambda^s}{c_p^s} \nabla h^s\right) = 0 \tag{5}$$

where the superscript s denotes the solid, ρ^s denoting the density, h^s the enthalpy, c_p^s the isobaric specific heat capacity, and λ_s the thermal conductivity of said solid.

The equations were solved using standard OpenFOAM algorithms with the Courant number, *Co*, being limited to 0.5. The Courant number is defined as:

$$Co = \frac{u \Delta t}{\Delta x} \tag{6}$$

Fixing the Courant number limited the time step, Δt, with the magnitude of the flow velocity in a certain direction, u, being calculated at each instance, and the length between cells in that direction, Δx, being fixed by the mesh resolution.

The models that are described next are critical components for any multiphase solver, and owing to the modularity of the *TwoPhaseFlow*

library they are easily interchangeable. The Volume of Fluid method utilised by the framework requires an advection scheme and a reconstruction scheme. The geometric Volume of Fluid method proposed by Roenby et al. [21] was employed, which uses a Piecewise Linear Interface Construction scheme for reconstruction of the interface [22].

The phase change module specifying mass flux across the interface between the vapour and liquid consists of a means of describing the saturation properties and an energy source term. Since the temperature ranges were very small, constant thermophysical properties were assigned to the fluid's liquid and vapour phases. A gradient based means was used to calculate the power associated with phase change:

$$q_{pc} = \lambda^l \nabla T^l \bullet \widehat{\boldsymbol{n}}_{int} + \lambda^l \nabla T^l \bullet (-\widehat{\boldsymbol{n}}_{int}) \tag{7}$$

The implicit gradient method proposed by Batzdorf [23] was used in this equation. The mass source term used was a modified Hardt and Wondra scheme [22], while the surface force module incorporated a Reconstructed Distance Function model based on Cummins et al. [24].

2.2. Numerical domain, boundary, and initial conditions

Since this study aimed to mimic real life applications, solid conjugation with a prescribed heat flux instead of temperature was considered critical. This also meant that a surface containing a single cavity would be insufficient, since the structural limitations on bubble growth, as well as possible conjugate effects on the thermal boundary layer of an uneven surface would not be captured fully.

While modeling a fully three-dimensional heat sink with varying machined surface patterns would be ideal, the constraints of time and computational power, as well as the vast scale differences restricted the domain size. The numerical domain (Fig. 1) consisted of an axisymmetric solid with a width and height of 0.0016 m, which was situated in a fluid of the same width of 0.0016 m and a height of 0.0048 m.

The y-axis at $x = 0$ m was the axis of symmetry, with the solid-to-fluid interface being situated at $y = 0$ m. This interface was set to be a no-slip velocity boundary condition, while a slip boundary condition was assigned at $x = 0.0016$ m. Simulations were first conducted using a smooth interface for validation and comparison purposes, and thereafter for set roughness topologies, as shown schematically in the figure. At the top of the domain ($y = 0.0048$ m) a pressure inlet/outlet velocity was prescribed. For the temperature boundary condition, it was assumed that adiabatic conditions prevailed at all surfaces but the interface, which was set to a simple coupled condition. At the bottom of the domain ($y = -0.0016$m) the solid was set to have a constant heat flux. As the heat flux was prescribed on an idealised smooth surface, and propagated through the thickness of the solid, a constant heat flux could be prescribed, disregarding the extended area necessitated by the roughened surfaces. Lastly, the pressure was set to a fixed flux at the interface and sides, with a total pressure condition being assigned to the top of the domain.

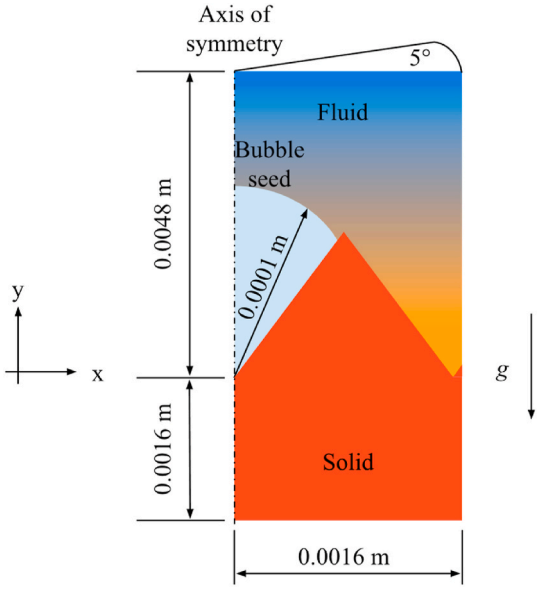

Fig. 1. Numerical domain illustrating the dimensions of the solid, fluid, and bubble seed.

Since a bubble nucleation model was not included in the solver, an initial seed bubble of radius $R_b = 100$ μm was placed at the origin ($x = 0$ and $y = 0$). The bubble centre was then raised by $0.67R_b$ to ensure that the prescribed contact angle was easily satisfied. A constant contact angle (not shown in the figure), $\theta = 54°$, was prescribed, based on the experimental observations by Li et al. [17] for smooth surfaces.

For the validation using a smooth surface, and the structured surface comparisons, a single-phase simulation was run with an initial saturation temperature of 25 °C throughout the domain for a set time to obtain the temperature field for each surface. This was then used as the initial temperature condition for the two-phase simulation. The single-phase simulation times were specifically chosen to ensure that the fluid region at a thickness of $y = 0.00025$ m and $x = 0$ m was at a superheat of 0.9 °C. This thickness was dictated by the Kays and Crawford [25] free convection equation:

$$\delta_{KC} = 7.14\left(\frac{\mu_l \alpha_l}{\rho_l g \beta_l (T_w - T_{sat})}\right) \tag{8}$$

where α_l is the thermal diffusivity of the liquid and β_l the thermal expansion coefficient of the liquid. This calculated distance varied between 0.00033 m and 0.00023 m depending on the imposed heat flux (and thus superheat). It was decided to keep this distance constant at 0.00025 m for ease of visual confirmation of the temperature and time in the visualisation software used.

2.3. Surface characterisation

This study focused on surfaces obtainable with simple manufacturing processes, such as by use of a lathe, as shown in Fig. 2. In this figure, each rotation of the lathe accounted for 120 μm in the lateral direction. This was used as a guideline to define surfaces with differing triangular topologies which could feasibly be achieved.

These topologies were chosen to investigate the effect of selecting differing incident cutting tool angles or different cutting speeds to finish a surface. The average surface roughness (R_a), defined as the arithmetic average profile height deviation from the mean line, is often used as an indication of surface finish. Referring to the scale in Fig. 2, and for comparison purposes, R_a was kept constant at 75 μm (meaning that the depth of cut was 150 μm). Selection of the angle at which the cutting tool

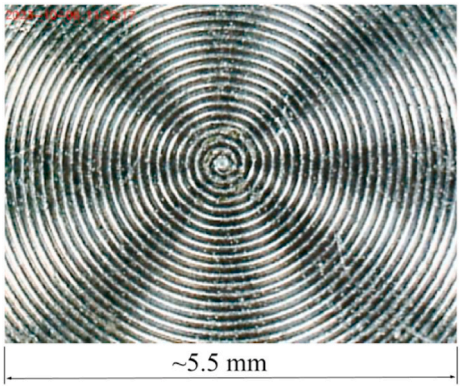

Fig. 2. Top down photograph of physical example of the proposed surface obtained using a lathe.

met the surface and the depth of cut meant that the indentation angle was fixed. This angle differed between the centre and the grooves because of a lathe's operation, but due to only a single bubble being investigated at the centre, this was deemed negligible. Five different triangular surface topologies were considered, each with a different indentation angle, as shown in Fig. 3. The vertical incident angle β was chosen to be 90°, 80°, 70°, and 60°, with the special case of the isosceles triangle having a value of β = 63°. With the value of R_a staying constant throughout, the resulting indentation angles α were 90°, 79°, 65°, and 46°, with the special isosceles case resulting in an indentation angle of 53°.

Since the problem was axisymmetric, it was limited to a single bubble at the origin, and thus a fully machined surface over the extent of the numerical domain width was not strictly necessary. An alternative approach was to limit the structured area of the surface to two or three grooves from the centre, with the remainder of the surface being smooth. In the interests of generality and completeness, however, the entire surface was considered as machined.

2.4. Numerical simulation matrix

The smooth surface and five machined surfaces were investigated using different wall heat fluxes and two refrigerants, as summarised in Table 1. For comparison purposes, the selection of refrigerants (R32 and R1234yf) and heat fluxes were based on the experimental values obtained from Li et al. [17]. The fluid properties of both refrigerants were obtained from CoolProp [26], and are compared at saturation

Table 1
Numerical simulation matrix.

Surface type	q [kW/m^2]					
	7.6	16	28	8.2	16	26
Smooth	R1234yf	R1234yf	R1234yf	R32	R32	R32
α = 90°	R1234yf	R1234yf	R1234yf	R32	R32	R32
α = 79°	R1234yf	R1234yf	R1234yf	R32	R32	R32
α = 65°	R1234yf	R1234yf	R1234yf	R32	R32	R32
α = 53°	R1234yf	R1234yf	R1234yf	R32	R32	R32
α = 46°	R1234yf	R1234yf	R1234yf	R32	R32	R32

Table 2
Physical properties of refrigerants at 25 °C.

Fluid	R32	R1234yf
P_{sat} [Pa]	1 689 621	682 582
ρ_l [kg/m^3]	961	1091
ρ_v [kg/m^3]	47	38
μ_l [Pa.s]	0.000112	0.000145
μ_v [Pa.s]	1.377	1.254
$c_{p,l}$ [J/kg°C]	1936	1392
h_{lv} [J/kg]	270 908	145 367
λ [W/m°C]	0.134	0.0636
α [m^2/s]	7.205×10^{-8}	4.181×10^{-8}
σ [N/m]	0.00679	0.00617

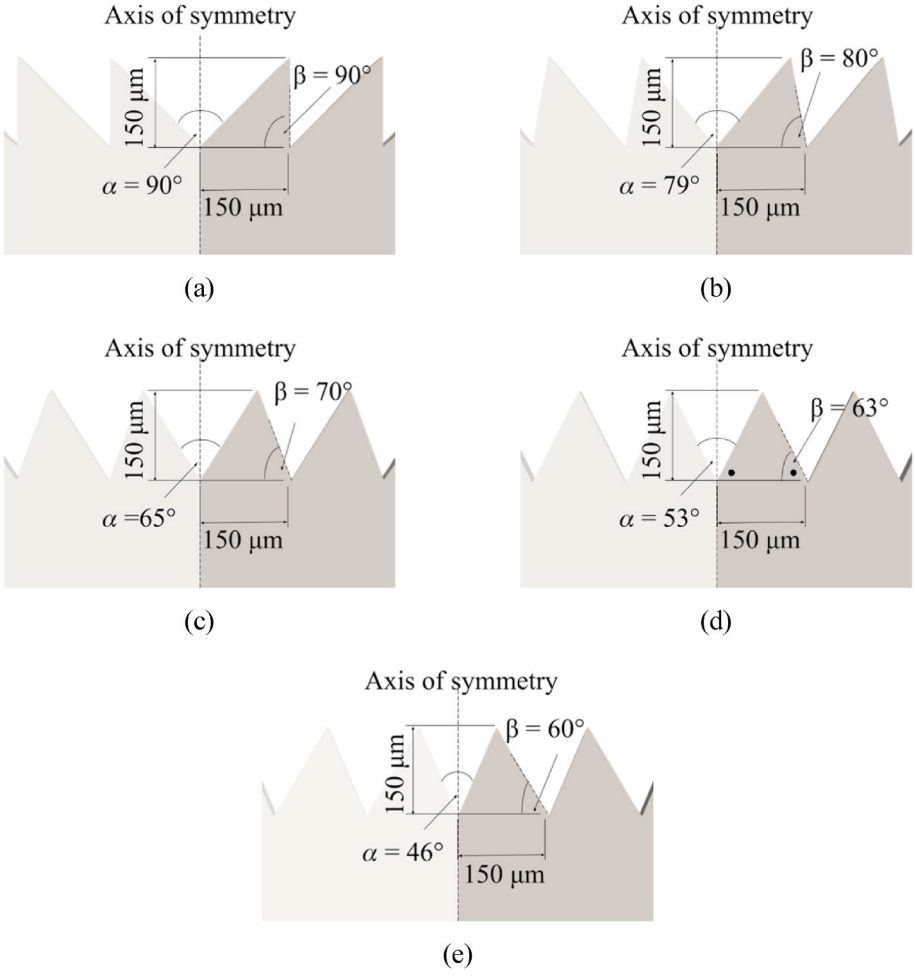

Fig. 3. Schematic of the machined surfaces considered in this study with a constant average surface roughness of 75 µm and indentation angle, α, equal to (a) 90°, (b) 79°, (c) 65°, (d) 53°, and (e) 46°.

temperature of 25 °C in Table 2. Although two refrigerants were tested, the results obtained using R32 were presented almost exclusively in this paper due to the similarities in the results.

2.5. Mesh dependence

To ensure the reliability of the results and analysis, the effect the grid size had on the solution had to be quantified. Ideally, mesh independence would be achieved once the calculated parameters no longer changed appreciably with additional mesh refinement. The initial conditions should have no effect on the results in the case of achieving a pseudo-steady state solution, but reaching this state requires many ebullition cycles of bubble growth and departure. To speed up solution times, a linear initial temperature field was prescribed. To ensure bubble growth, this field ranged from a superheated surface temperature of 28.6 °C at $y = 0$, up to the saturation temperature of 25 °C at a semi-arbitrary distance of $y = 0.00346$ m. This surface temperature was obtained from the experimental values by Li et al. [17].

Since this study was concerned with bubble dynamics, the chosen parameter for this dependency test was the equivalent bubble diameter, D_{eq}. This value was calculated by outputting the bubble volume and, during postprocessing, setting it equal to the volume of a sphere, from which the equivalent diameter could be obtained:

$$D_{eq} = \left(\frac{6V_{bub}}{\pi}\right)^{\frac{1}{3}} \tag{9}$$

where V_{bub} is the volume of the bubble output by an OpenFOAM postprocessing function. The specific case chosen for the mesh dependence study was that of the bubble growth of R32 on a smooth surface with a constant wall heat flux of 16 kW/m^2, with the remaining initial and boundary conditions as described in Section 2.2.

The meshes were structured and approximately square, with a uniform mesh resolution throughout the domain. To construct the meshes, a combination of tools was used. First, the interface was constructed in the software tool *Gmsh* [27] and exported as an STL file. This file was loaded into *snappyHexMesh*, an OpenFOAM meshing tool, which was then applied to map a structured mesh to the solid, taking the interface between the solid and fluid into account.

An example of the coarsest mesh on a smooth surface with a resolution of 56 μm was chosen as baseline and compared with the results of successively finer resolutions of 32, 24, 20, and 16 μm. The number of cells for each of these resolutions is summarised in Table 3, with the bubble growth results compared in Fig. 4.

It follows from Fig. 4 that increasing the mesh resolution results in an increased bubble growth and departure rate. Bubble departure is indicated by the equivalent diameter becoming constant at approximately 0.001 m, with the sudden sharp drop indicating that the bubble has left the numerical domain. The difference in equivalent diameter as a function of time between the two finest meshes (resolutions of 16 and 20 μm) considered was only 2.6 %. While it was possible to increase the accuracy further by introducing smaller mesh resolutions, the solution times would become untenable without a substantial increase in solution accuracy. Initial simulations with a mesh of 32 μm resolution resulted in a wall-clock time of approximately 3600 s to solve 1.5 s of bubble growth. Halving the resolution to 16 μm, resulted in a four-fold increase in the number of elements, with a concomitant almost four-fold

Table 3
Mesh resolution and number of cells.

Mesh resolution (μm)	Number of cells
56	3335
32	10 200
24	17 889
20	25 600
16	40 400

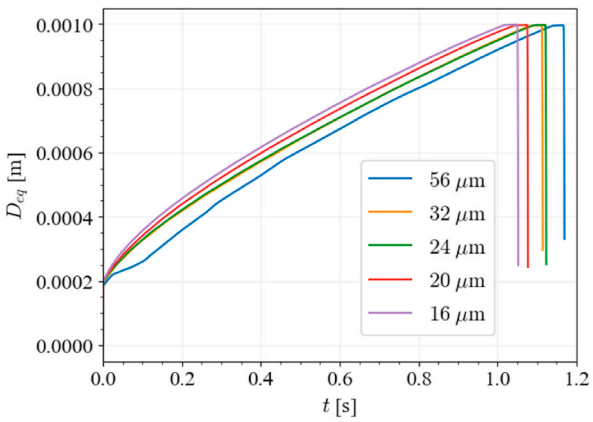

Fig. 4. Mesh dependence study for bubble growth of R32 on a smooth surface at a heat flux of 16 kW/m^2.

increase in the time taken to solve, in this case approximately 13 000 s. Halving this resolution to 8 μm resulted in wall-clock times in excess of 50 000 s, and it was therefore decided that the 16 μm mesh resolution was sufficient for this study.

For the smooth surface, no problems were encountered with meshing. However, the sharp points in the different topologies envisaged in Fig. 3, made it excessively hard to obtain a mesh that did not result in diverging solutions. After extensive modification of the parameters in the *snappyHexMesh* tool, meshes which produced non-divergent results were successfully generated for all the topologies that were to be investigated. An example of this type of mesh, constructed for the topology in Fig. 3(d), is shown in Fig. 5.

2.6. Validation

With the mesh resolution selected, attention was turned to validating the bubble growth and departure rates. Although many studies investigated nucleate pool boiling on smooth surfaces and single cavities, to the authors' best knowledge, no prior investigations considered the microstructures investigated in this study. Therefore, the validation was conducted using a smooth surface by comparing the results with the experimental data of Li et al. [17] for R32 at a heat flux of 16 kW/m^2, as well as the correlation by Sakashita [19] in Fig. 6.

The same method used by Li et al. [17] was used to obtain the equivalent diameters and careful attention was paid to ensure that the

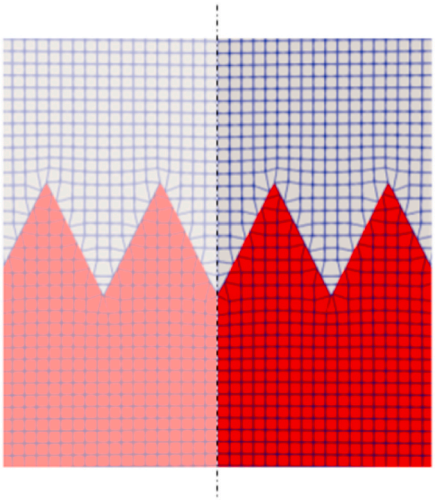

Fig. 5. Sample of a non-divergent mesh for β = 63°obtained with *snappyHexMesh*.

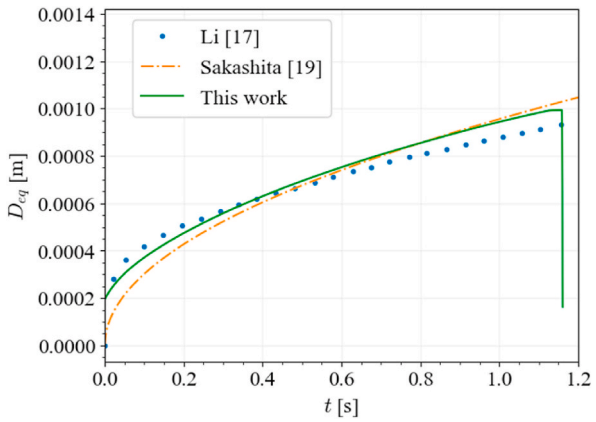

Fig. 6. Validation of numerical work by comparison to experimental data [17] and analytical predictions [19] for R32 at a heat flux of $q = 16$ kW/m^2.

experimental conditions were reproduced, such as the applied heat flux which was obtained directly from the authors. From this figure it becomes apparent that the numerical approach was valid, with the bubble diameter as a function of time showing a mean absolute error of 6 % when compared to the experimental values, and a mean absolute error of 9 % when compared to the correlation of Sakashita [19]. The bubble growth time until departure was also within 0.2 % of the experimental data. When comparing the departure diameter with the experimental data, it was higher by 6.6 %, but considering the low mean absolute error and departure time error, this was deemed acceptable.

3. Results

First, a qualitative investigation was done to gauge the effect of the different surface topologies at a specific wall heat flux before an in-depth force analysis was done to investigate the bubble departure. This led to a comparison of the simulation results of the entire machined surface with only a single indentation of the same topology.

3.1. Qualitative effect of surface topology on bubble dynamics for multiple heat fluxes

The bubble growth curve and departure time for R32 over varying surfaces for heat fluxes of 8, 16, and 26 kW/m^2 are shown in Fig. 7. The surface topology had a definite impact on bubble dynamics, as expected, although some of the results were surprising. In general, the bubble behaviour for the surfaces were similar for all heat fluxes, and independent of the refrigerant. It follows from Fig. 7(a) that a decrease in indentation angle resulted in faster bubble departure. Furthermore, as has been found by previous experimental studies [28,29], an increased heat flux also resulted in a faster bubble departure. The departure diameter remained largely unaffected by the increasing heat flux for any surface.

Of interest is the fact that the bubble growth rate for any indentation angle less than 90° was almost exactly the same, with only the departure time and thus departure diameter differing. The growth rate was slower than for a smooth surface. This agrees with extant literature [30,31] in that the diameter is proportional to time raised to an exponent n, multiplied with a proportionality constant. The structured surfaces inevitably caused the bubble to have less contact area with the heated surface and disrupted the thermal boundary layer which delayed the growth compared to the smooth surface. However, this decreased bubble growth rate (and thus decreased heat removal rate) was balanced by the higher bubble departure frequency for indentation angles below a critical value, as discussed below.

To further investigate and quantify the effects of indentation angle and heat flux on departure diameter and time for the different surfaces,

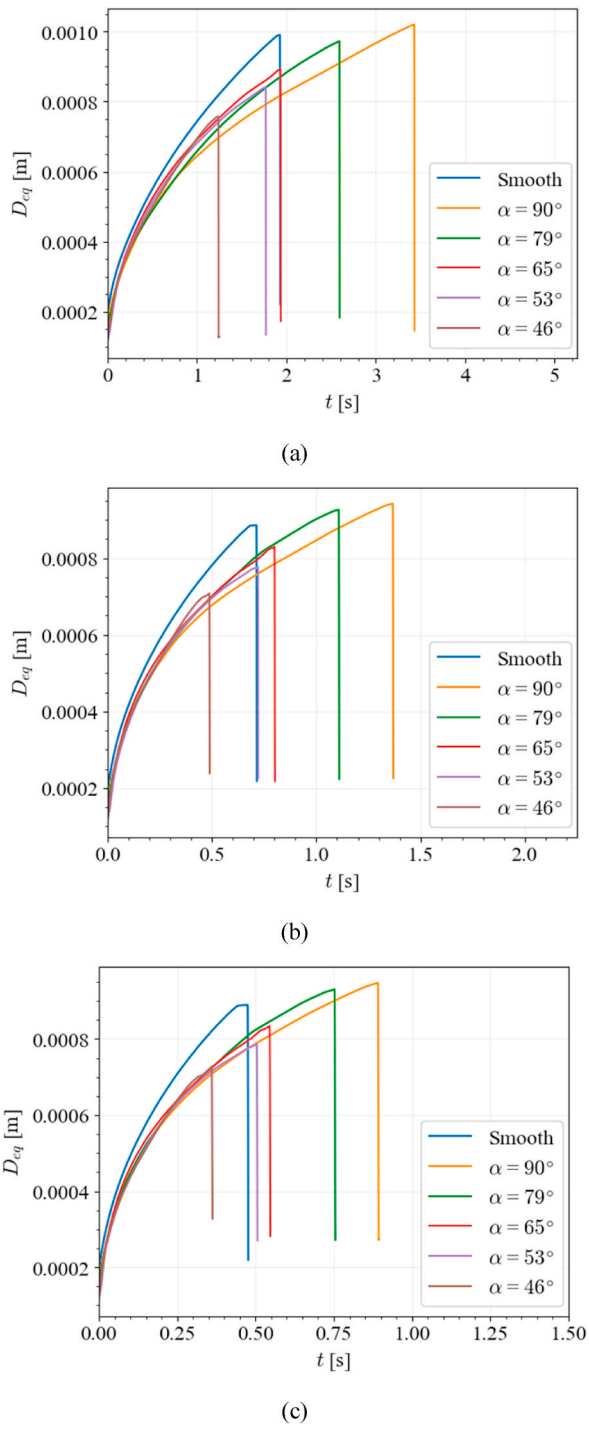

Fig. 7. Bubble growth on various surfaces for R32 at (a) $q = 8$ kW/m^2, (b) $q = 16$ kW/m^2, and (c) $q = 26$ kW/m.^{2}.

the departure diameter and time have been normalised with respect to the smooth surface and compared as a function of indentation angle in Fig. 8. From the solid circle markers in this figure, it follows that indentation angles of 90° and 79° had very little influence on departure diameter, while the cross markers indicate that it had a marked effect on departure time, being in excess of 130 % of that of the smooth surface.

As the indentation angle decreased to 53° and 65°, the departure time approached that of the smooth surface, with the departure diameter being between 85 % and 90 % of the smooth surface. For an indentation angle of 46°, however, the departure diameter and time decreased significantly. The diameter was approximately 75 % of the

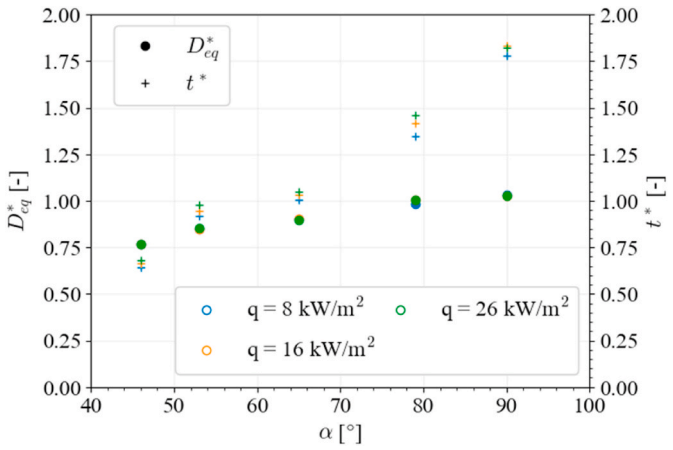

Fig. 8. Normalised departure diameters and times with respect to a smooth surface for R32 as a function of indentation angle for multiple heat fluxes.

smooth surface, with the time being 70 %. These results indicated that a critical indentation angle existed above which only the departure time was affected and below which both the departure diameter and time were affected. The critical angle appeared to be approximately 60° for the machined surfaces investigated in this study, but can be refined through additional studies on a wider range of surfaces.

To compare the trends for different refrigerants, Fig. 9 compares the bubble growth of R32 and R1234yf for different indentation angles at a heat flux of 16 kW/m^2. As can be seen, the qualitative behaviour of R1234yf was very similar to that of R32 and different departure times and diameters were caused by the difference in fluid properties. The enthalpy of vaporisation for R1234yf is much lower than that of R32, as seen in Table 2, which was why at the same heat flux the bubble diameter for R1234yf was larger at a specific time. The density of R1234yf is also lower than that of R32, and this was visible in the decreased departure time. The results obtained using R1234yf will not be presented and discussed in detail.

3.2. Force analysis for smooth and machined surfaces

It was concluded from Figs. 7 and 8 that the bubble dynamics were largely influenced by the surface topology, with opposite trends in departure time being exhibited when comparing the extremes of the indentation angles. To gain an improved understanding of the effect of surface topology on bubble growth and departure time, a force analysis

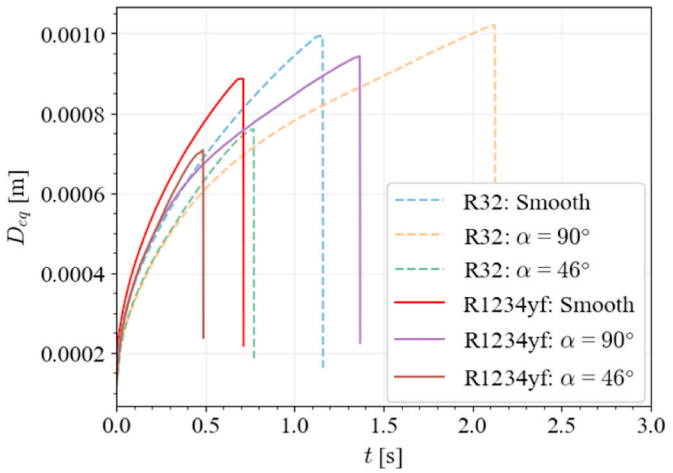

Fig. 9. Comparison between the bubble growth of R32 and R1234yf results for different surfaces at a heat flux of 16 kW/m^2.

was performed, taking into account the major forces acting on the bubble in the vertical direction.

The dominating forces were the buoyancy force, F_B, the pressure force, F_P, and the surface tension force, F_S. While other forces, including drag, added mass, and gas momentum also played a role in the bubble growth, the growth rate was considered too low for these to have an undue influence. Boubendir et al. [32] concluded the under quasi-static conditions, only the buoyancy, pressure, and surface tension forces were important. Mahmoud and Karayiannis [33] found that for boiling water, the vapour inertia, drag, and lift forces could be neglected, and that beyond the initial bubble formation time of about 4 ms, the pressure, surface tension, and buoyancy forces dominated. As such, a schematic of these forces is shown in Fig. 10, with the convention that attaching forces (F_S) are in the negative direction, while detaching forces (F_B and F_P) are positive.

The buoyancy force was calculated as follows:

$$F_B = (\rho_l - \rho_v) g V_{bub} \tag{10}$$

where V_{bub} is the volume of the bubble. To calculate the pressure force, a similar approach to Boubendir et al. [32] was followed:

$$F_P = (P_v - P_l) \frac{\pi}{4} D^2_{base} \tag{11}$$

where P_i is the appropriate liquid or vapour pressure, and D_{base} is the dry patch diameter. This agrees with extant literature in that the area of the dry patch plays an important role in calculating the pressure force. Mahmoud and Karayiannis [33], for example, calculated the pressure force using the area of the dry patch combined with the surface tension and actual bubble radius. The surface tension force was calculated using:

$$F_S = \pi D_{base} \sigma \sin\theta \tag{12}$$

where σ is the surface tension and θ is the contact angle. Finally, F_{net} is the sum of the three contributing forces:

$$F_{net} = F_B + F_P - F_S \tag{13}$$

Since the qualitative results from Fig. 7 were very similar, only two surfaces from Fig. 7(b) were selected: (1) indentation angle of 79°, which showed delayed bubble departure time, and (2) indentation angle of 46°, which showed the opposite trend. The force evolutions recorded for these two surfaces are compared in Fig. 11. To show the effect of the forces and surface topology on the bubble growth, the non-dimensionalised base diameter, D^*_{base}, is also included. This diameter was non-dimensionalised by the initial base diameter cavity diameter for the smooth surface and by the cavity diameter for the structured rough surfaces. For clarification in subsequent discussions, the initial bubble growth stage is marked by the symbol *A*, the maximum base diameter by *B*, and the point of necking and departure by *C*.

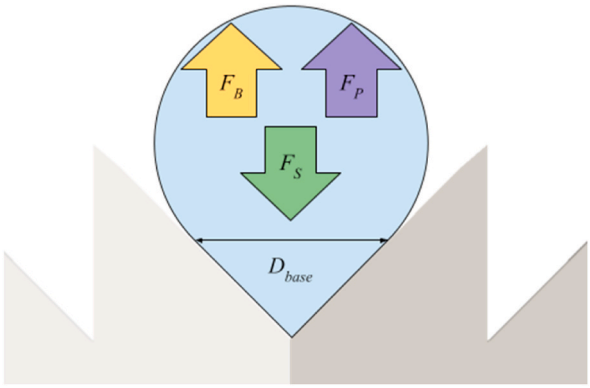

Fig. 10. Force diagram of a growing bubble indicating the attaching (F_S) and detaching forces (F_B and F_P).

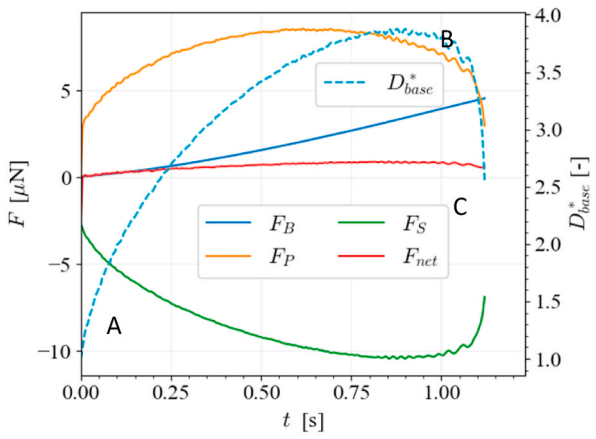

(a)

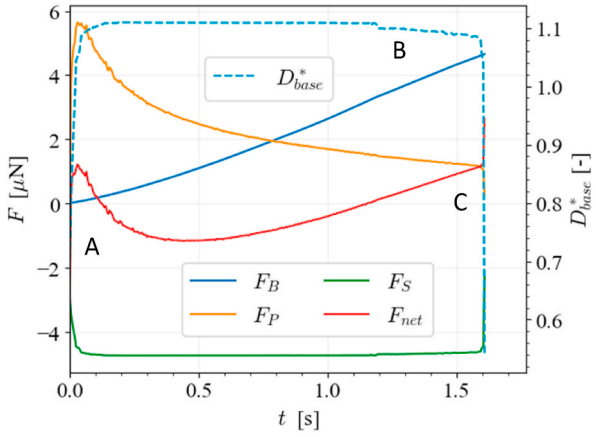

(b)

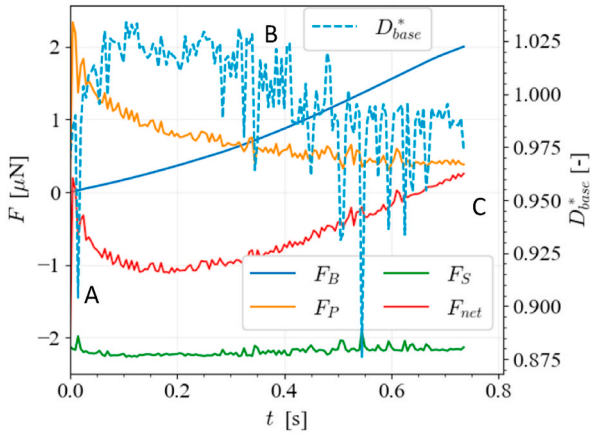

(c)

Fig. 11. Force evolution and base diameter for a growing R32 bubble with heat flux 16 kW/m^2 for (a) a smooth surface, (b) an indentation angle of 79°, and (c) an indentation angle of 46°.

It follows from Fig. 11(a) that for a smooth surface, the surface tension continually increased as there was no limitation on the expansion of the bubble. It plateaued at roughly $t = 0.8$ s, where the base diameter was no longer increasing. In opposition, the pressure force grew with the base diameter, as did the buoyancy force with the volume of the bubble. When the buoyancy and pressure forces exceeded the surface tension force, the base diameter in contact with the surface suddenly contracted and the bubble departed. The net force line was relatively stable around the zero line for the smooth surface. The net force line was positive before bubble departure and deviated only slightly from zero, indicating that the additional adhesive forces, although active, did not play a major role in the force balance. It was thus concluded that the accuracy of the solution was not significantly influenced by only considering the forces shown in Fig. 10.

When comparing the results of the smooth surface to the structured surfaces for indentation angles of 79° (Fig. 11(b)) and 46° (Fig. 11(c)), it follows that the maximum surface tension force was reached almost immediately, and remained constant for the entire growth period until bubble departure. When the non-dimensionalised diameter was considered, the reason for this became apparent. Since the initial bubble diameter was somewhat smaller than the cavity diameter in Fig. 11(b), D^*_{base} started at a value less than unity. The bubble grew until it reached a D^*_{base} value of approximately unity, after which the base diameter ceased growing. The cavity diameter and the initial bubble diameter were approximately equal for Fig. 11(c), meaning D^*_{base} started at a value of unity and did not increase. This implied that the bubble in contact with the heating surface could not physically grow due to the structural limits imposed by the machined surfaces. This necessarily meant the surface tension and pressure force were limited as well. The value in excess of unity for D^*_{base} in Fig. 11(b) was due to the base diameter being defined as the position where the phase fraction was zero (fully liquid). Due to the diffusive effects of the volume of fluid method and the mesh size selected, this was slightly beyond the cavity radius. The oscillation visible in Fig. 11(c) was due to the bubble radius being on the same scale as that of the mesh size, amplifying minor fluctuations. These problems were unexpected, and can be avoided in future by implementing a finer mesh and decreasing the radius of the bubble seed.

This physical limitation in bubble base diameter can also explain why the bubble departure time was slower for the indentation angle of 79° and faster for the angle of 46°. The equivalent diameter (and thus the volume and buoyancy force) grew at approximately the same rate for all surfaces, as seen in Fig. 7. However, since the surface tension force was limited by the achievable base diameter, which was much smaller for the angle of 46°, the net force quickly became positive, resulting in bubble departure.

On the other hand, for the angle of 79°, the maximum surface tension force was reached quickly and maintained, but the pressure force was reduced to such an extent that the buoyancy force had to overcome the downwards force on its own for detachment to happen. For the smooth surface, the base diameter was unconstrained and the surface tension force was larger, but the pressure force was also larger which aided the buoyancy and resulted in a faster departure time than for a shallow indentation angle surface.

3.3. Comparison of bubble dynamics between structured surfaces and single cavities

Many experimental studies focused on single bubble dynamics on a smooth surface [33,34] or from a single artificial nucleation site [17,35] to control bubble nucleation. Many numerical studies followed the same route [18,36,37], while others aimed to elucidate the interaction between neighbouring bubbles [38]. It is worth noting that a fully structured surface, as would be encountered at application level, was not investigated in previous studies. Since bubble growth is not physically constrained in these investigations, the results are different when compared to a fully structured surface. Depending on the goal of the study, it may be critical to consider a fully structured surface, even if only single bubble growth is being evaluated.

This was borne out by Fig. 12, in which the bubble growth results of single cavities of the same indentation angle as the fully structured surface were compared. This figure indicates that the single cavities exhibited much closer results to the ideal perfectly smooth surface than the fully structured surfaces. Similar departure diameters were obtained

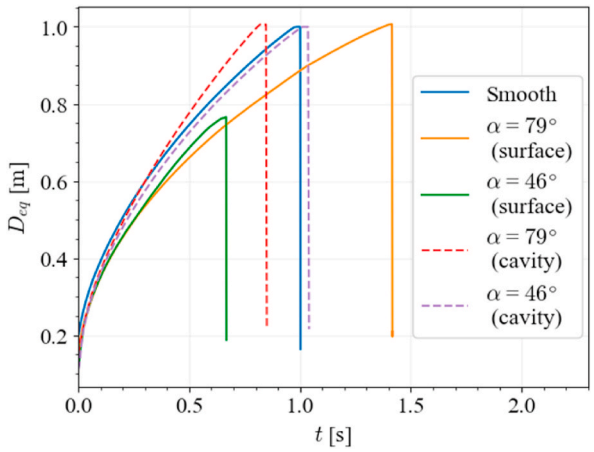

Fig. 12. Comparison of bubble growth between fully structured surfaces and single cavities for indentation angles 79° and 46° with a heat flux of 16 kW/m^2.

with minor deviations in the bubble growth rate. For the fully structured surface, the growth rates were slightly less than for the smooth and single cavity results, while the departure diameter and time were significantly affected by the indentation angle. This was due to the physical limitation on the bubble size and the limits imposed on the major forces, as discussed in Section 3.2.

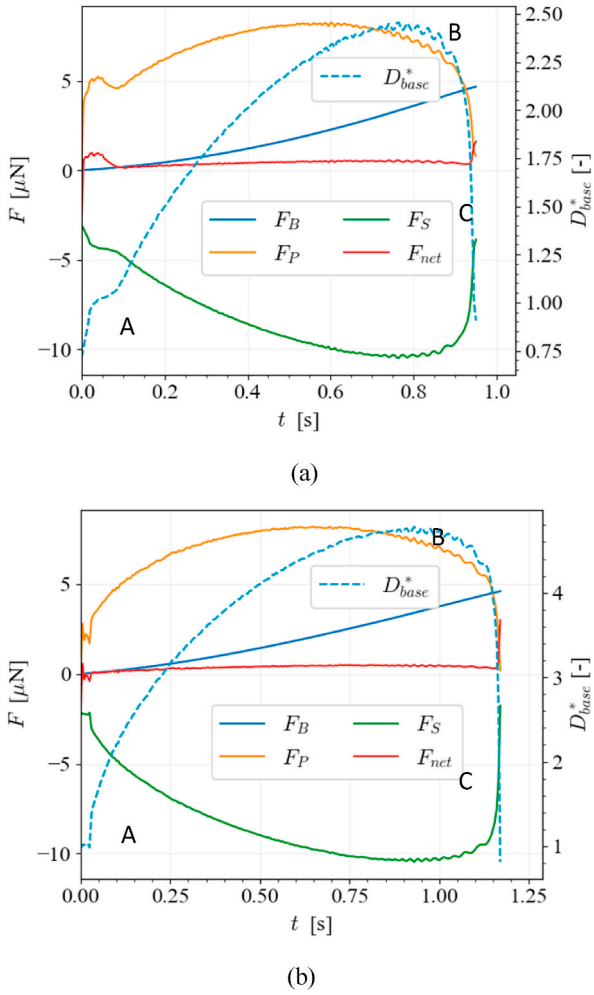

Fig. 13. Force evolution and base diameter of a growing R32 bubble with heat flux of 16 kW/m^2 for a single cavity with (a) an indentation angle of 79°, and (b) an indentation angle of 46°.

To cement the idea that bubble size limitations should be one of the main factors considered in future studies, the force balance diagrams for the single cavities are shown in Fig. 13, with the diameters non-dimensionalised with the cavity diameters. When comparing this to the smooth surface in Fig. 11(a), the similarities are self-evident. For the cavity with an indentation angle of 79° in Fig. 13(a), the bubble seed, which was smaller than the radius of the cavity, grew steadily until a time of approximately 0.05 s, at which point the growth was paused until 0.01 s. This is the timeframe in which the bubble reached the cavity lip, and once the bubble overcame that lip, it continued growing similar to the bubble growth on a smooth surface. The same behaviour can be observed in Fig. 13(b), where the bubble seed radius equalled the cavity radius immediately, and once the lip was overcome, the bubble growth proceeded similar to the smooth surface.

The bubble growth for smooth surfaces, single cavities and structured surfaces are compared visually in Fig. 14 for refrigerant R32. The bubble growth stages are labelled A (initial bubble growth), B (maximum base diameter), and C (necking), as in Figs. 11 and 13. The time at which the observations were made are included below each image, while the normalised times (with respect to the departure time) are given in brackets.

As expected, the initial stages were similar for all surfaces. For the single cavities, the maximum value of the base diameter was almost exactly the same as that for the smooth surface. The structured surfaces, however, limited the maximum base diameter. This was most prominent in the structured surface with an indentation angle of 46°, where the bubble grew in a spherical shape, as opposed to the ellipsoidal shape of the other surfaces. The remaining images shown for necking are snapshots of the bubble just before departure. Since the output time was not set to a fine enough level, being 0.005 s, the necking was not fully visible for the smooth surface or the cavity with an indentation angle of 46°. For both the cavity and surface with indentation angle of 79° the necking behaviour looked similar, although no firm conclusions could be drawn from the results without refining the output times.

Bubble dynamics is of prime importance for heat transfer purposes. If one focused on bubble departure time and critical heat flux, the results investigated in this study seem to lead to a simple conclusion that more acute indentation angles resulted in shorter bubble departure times, leading to improved critical heat fluxes. Future investigations can thus be limited to indentation angles of 46° and below. However, the physical limitations on bubble size of the fully machined surface also limit the possible heat transfer due to surface rewetting which scales with the difference between maximum and minimum bubble base radius. Other factors also play important roles in bubble dynamics and heat transfer. For example, the uniformity of departure frequency and departure diameter both play a major role in the stability of heat transfer, which is critical for electronics cooling. Vapour retention, eliminating the waiting time for bubble nucleation, was not investigated in this work, since only a single bubble departure was modelled. Furthermore, running several ebullition cycles can provide in-depth understanding of the bubble generation, growth, and detachment.

4. Conclusions

The need for a cost-effective, easy to implement method of enhancing and controlling the nucleate boiling process and bubble dynamics, along with the need to gain greater understanding into the bubble behaviour was recognised. To this end, the potential of using a lathe to manufacture structured surfaces for heat sinks was investigated numerically for R32 and R1234yf, two refrigerants being considered for immersion cooling. Conjugate heat transfer in a multiphase library for OpenFOAM was utilised, and a structured mesh of element size 16 μm was used. The structured surfaces, obtained using a combination of tools, had different indentation angles but a constant average roughness of 75 μm. These structures were compared to a smooth surface, as well as

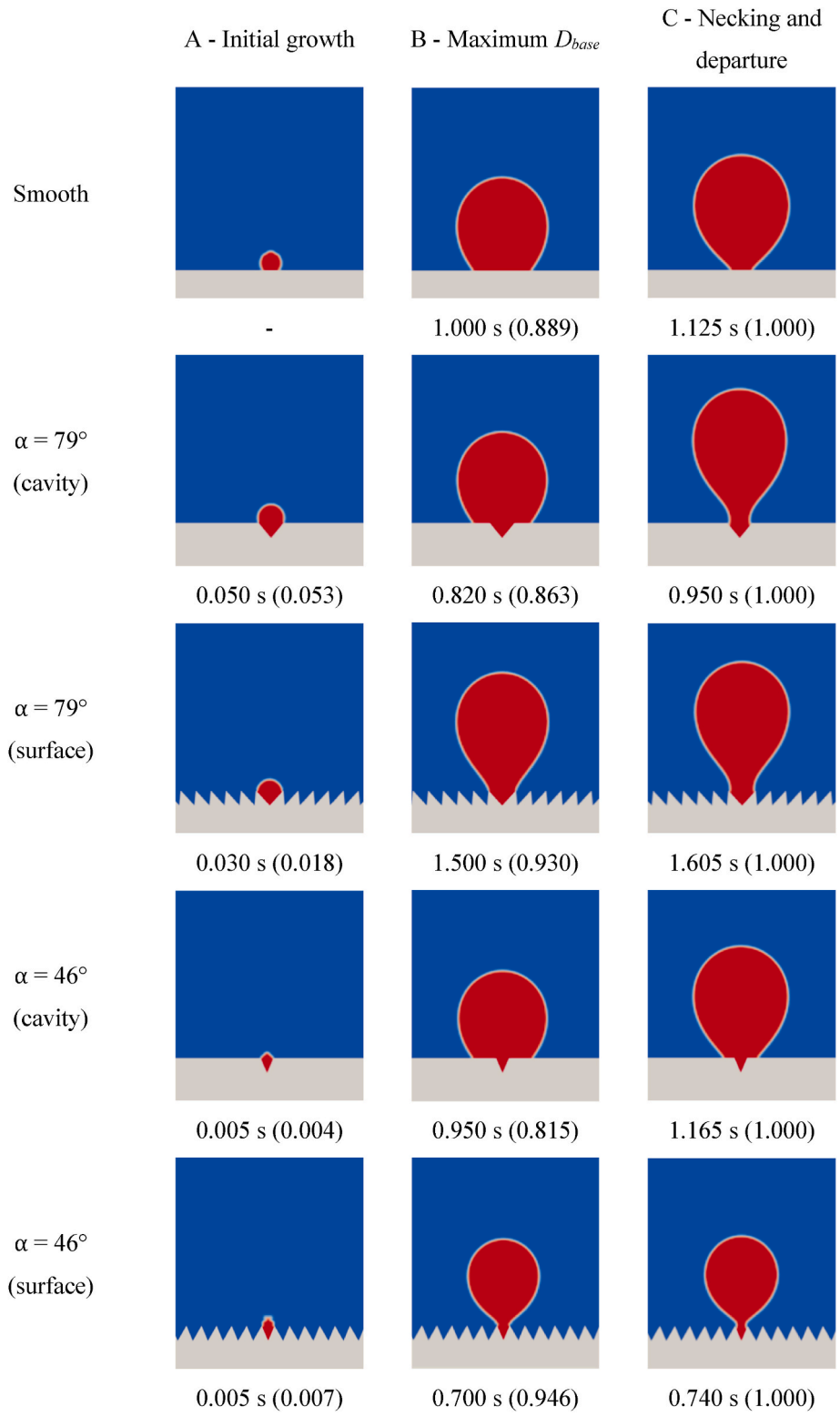

Fig. 14. Bubble growth comparison between smooth, structured, and single cavity surfaces for R32 with heat flux 16 kW/m^2. The time at which the observations were made are included below each image, while the normalised times (with respect to the departure time) are given in brackets.

a smooth surface with a single cavity and comparable indentation angles.

Qualitatively, it was observed that the bubble growth curves showed similar behaviour at heat fluxes ranging from 7.6 kW/m^2 to 28 kW/m^2 for R32 and R1234yf. The growth rate was slower than the smooth surface, but approximately the same for all indentation angles less than 90°. The equivalent diameter and time, normalised with respect to a smooth surface, showed that the departure diameter was independent of heat flux. The departure time for indentation angles of 90° and 79° was upwards of 130 % than that of the unmodified surface, while the departure diameters for these indentation angles were very similar to the smooth surface. For indentation angles of 65° and 53°, the departure

time was similar to the smooth surface, with the departure diameter being approximately 85 %–90 % of that of the smooth surface. The departure diameter and time for an indentation angle of 46° were 75 % and 70 % of those of the smooth surface, respectively. The critical angle at which bubble dynamics showed this shift in bubble departure time and diameter was approximately 60°, although it can be refined through further investigation.

A force analysis led to the conclusion that the bubble growth being physically inhibited by the structured surfaces was responsible for both the delayed and accelerated departure time of the bubble. To investigate and confirm the major effect this pinning of the bubble at the edge of the structured roughness had, a comparison with the more traditional single cavity study was also conducted. These single cavity tests exhibited similar behaviour to that of the smooth surface, and differed widely from the structured surfaces. This confirmed that testing a surface that is machined beyond just the bubble nucleation cavity, either numerically or experimentally, plays a critical part in evaluating surfaces that will eventually be used in practice. For practical implementation, a shorter bubble departure time is desirable to delay the onset of critical heat flux, and thus an indentation angle of below 46° was suggested for further study.

Additional work is needed to illustrate multiple bubble interactions, uniform bubble departure size, and stable frequency of bubble departure. In order to facilitate meshing and reduce computational requirements, a structured surface containing smoother edges and only the minimal amount of grooves that would limit bubble size can be adopted in future.

CRediT authorship contribution statement

W.J. van den Bergh: Writing – original draft, Visualization, Validation, Software, Methodology, Investigation, Formal analysis, Data curation, Conceptualization. **M. Whiting:** Writing – review & editing, Software. **P.E. Theodorakis:** Writing – review & editing, Supervision, Resources, Funding acquisition. **M. Everts:** Writing – review & editing, Supervision, Project administration, Funding acquisition, Conceptualization.

Declaration of competing interest

The authors declare that they have no known competing financial interests or personal relationships that could have appeared to influence the work reported in this paper.

Data availability

Data will be made available on request.

Acknowledgements

This project has received funding from the European Union's Horizon 2020 Research and Innovation programme under the Marie Skłodowska-Curie grant agreement no. 778104.

We also gratefully acknowledge the Polish high-performance computing infrastructure PLGrid (HPC Centers: ACK Cyfronet AGH, WCSS) for providing computer facilities and support within the computational grant no. PLG/2023/016280.

References

[1] R.L. Mohanty, M.K. Das, A critical review on bubble dynamics parameters influencing boiling heat transfer, Renew. Sustain. Energy Rev. 78 (2017) 466–494.
[2] J.P. McHale, S.V. Garimella, Bubble nucleation characteristics in pool boiling of a wetting liquid on smooth and rough surfaces, Int. J. Multiphas. Flow 36 (4) (2010) 249–260.
[3] A. Suszko, M.S. El-Genk, Saturation boiling of PF-5060 on rough Cu surfaces: bubbles transient growth, departure diameter and detachment frequency, Int. J. Heat Mass Tran. 91 (2015) 363–373.
[4] D. Jung, et al., Nucleate boiling heat transfer coefficients of pure halogenated refrigerants, Int. J. Refrig. 26 (2) (2003) 240–248.
[5] S. Bovard, et al., Investigation and experimental analysis of the bubble departure diameter in pure liquids on horizontal cylindrical heater, Heat Mass Tran. 53 (4) (2017) 1199–1210.
[6] A. Inbaoli, C.S. Sujith Kumar, S. Jayaraj, A review on techniques to alter the bubble dynamics in pool boiling, Appl. Therm. Eng. 214 (2022) 118805.
[7] S.A. Khan, M.A. Atieh, M. Koç, Micro-nano scale surface coating for nucleate boiling heat transfer: a critical review, Energies 11 (11) (2018) 3189.
[8] A.M. Gheitaghy, H. Saffari, G.Q. Zhang, Effect of nanostructured microporous surfaces on pool boiling augmentation, Heat Tran. Eng. 40 (9–10) (2019) 762–771.
[9] P. Xu, Q. Li, Y. Xuan, Enhanced boiling heat transfer on composite porous surface, Int. J. Heat Mass Tran. 80 (2015) 107–114.
[10] Y. Li, et al., Manipulating the heat transfer of pool boiling by tuning the bubble dynamics with mixed wettability surfaces, Int. J. Heat Mass Tran. 170 (2021) 120996.
[11] J. Wang, M. Diao, X. Liu, Numerical simulation of pool boiling with special heated surfaces, Int. J. Heat Mass Tran. 130 (2019) 460–468.
[12] Y. Song, et al., Enhancement of boiling with scalable sandblasted surfaces, ACS Appl. Mater. Interfaces 14 (7) (2022) 9788–9794.
[13] V.V. Nirgude, S.K. Sahu, Enhancement of nucleate boiling heat transfer using structured surfaces, Chem. Eng. Process: Process Intensif. 122 (2017) 222–234.
[14] H. Honda, J.J. Wei, Enhanced boiling heat transfer from electronic components by use of surface microstructures, Exp. Therm. Fluid Sci. 28 (2) (2004) 159–169.
[15] J.J. Wei, H. Honda, Effects of fin geometry on boiling heat transfer from silicon chips with micro-pin-fins immersed in FC-72, Int. J. Heat Mass Tran. 46 (21) (2003) 4059–4070.
[16] H. Scheufler, J. Roenby, TwoPhaseFlow: an OpenFOAM Based Framework for Development of Two Phase Flow Solvers, 2021 arXiv preprint arXiv:2103.00870.
[17] J. Li, Z. Yang, Y. Duan, Experimental study on single bubble growth of R32 + R1234yf binary mixtures during saturated pool boiling, Appl. Therm. Eng. 219 (2023) 119535.
[18] J. Li, Z. Yang, Y. Duan, Numerical simulation of single bubble growth and heat transfer of R32+R1234yf binary mixtures during saturated pool boiling, Int. J. Therm. Sci. 191 (2023) 108380.
[19] H. Sakashita, Bubble growth rates and nucleation site densities in saturated pool boiling of water at high pressures, J. Nucl. Sci. Technol. 48 (5) (2011) 734–743.
[20] J. Kim, Review of nucleate pool boiling bubble heat transfer mechanisms, Int. J. Multiphas. Flow 35 (12) (2009) 1067–1076.
[21] J. Roenby, H. Bredmose, H. Jasak, A computational method for sharp interface advection, R. Soc. Open Sci. 3 (11) (2016) 160405.
[22] S. Hardt, F. Wondra, Evaporation model for interfacial flows based on a continuum-field representation of the source terms, J. Comput. Phys. 227 (11) (2008) 5871–5895.
[23] S. Batzdorf, Heat transfer and evaporation during single drop impingement onto a superheated wall, in: Maschinenbau, Technische Universität: Darmstadt, 2015.
[24] S.J. Cummins, M.M. Francois, D.B. Kothe, Estimating curvature from volume fractions, Comput. Struct. 83 (6) (2005) 425–434.
[25] W.M. Kays, M.E. Crawford, B. Weigand, Convective Heat and Mass Transfer, fourth ed., McGraw-Hill series in mechanical engineering, Boston, 2005. McGraw-Hill Higher Education Boston.
[26] I.H. Bell, et al., Pure and pseudo-pure fluid thermophysical property evaluation and the open-source thermophysical property library CoolProp, Ind. Eng. Chem. Res. 53 (6) (2014) 2498–2508.
[27] C. Geuzaine, J.-F. Remacle, Gmsh: a 3-D finite element mesh generator with built-in pre- and post-processing facilities, Int. J. Numer. Methods Eng. 79 (11) (2009) 1309–1331.
[28] M. Gong, et al., Visualization study on nucleate pool boiling of ethane, isobutane and their binary mixtures, Exp. Therm. Fluid Sci. 51 (2013) 164–173.
[29] L.-H. Chien, R.L. Webb, Measurement of bubble dynamics on an enhanced boiling surface, Exp. Therm. Fluid Sci. 16 (3) (1998) 177–186.
[30] N. Zuber, The dynamics of vapor bubbles in nonuniform temperature fields, Int. J. Heat Mass Tran. 2 (1) (1961) 83–98.
[31] R. Cole, H.L. Shulman, Bubble growth rates at high Jakob numbers, Int. J. Heat Mass Tran. 9 (12) (1966) 1377–1390.
[32] L. Boubendir, S. Chikh, L. Tadrist, On the surface tension role in bubble growth and detachment in a micro-tube, Int. J. Multiphas. Flow 124 (2020) 103196.
[33] M.M. Mahmoud, T.G. Karayiannis, Bubble growth on a smooth metallic surface at atmospheric and sub-atmospheric pressure, Int. J. Heat Mass Tran. 209 (2023) 124103.
[34] H.C. Lee, et al., Single bubble growth in saturated pool boiling on a constant wall temperature surface, Int. J. Multiphas. Flow 29 (12) (2003) 1857–1874.
[35] S. Siedel, S. Cioulachtjian, J. Bonjour, Experimental analysis of bubble growth, departure and interactions during pool boiling on artificial nucleation sites, Exp. Therm. Fluid Sci. 32 (8) (2008) 1504–1511.
[36] Y.-T. Mu, et al., Nucleate boiling performance evaluation of cavities at mesoscale level, Int. J. Heat Mass Tran. 106 (2017) 708–719.
[37] S. Gong, P. Cheng, X. Quan, Two-dimensional mesoscale simulations of saturated pool boiling from rough surfaces. Part I: bubble nucleation in a single cavity at low superheats, Int. J. Heat Mass Tran. 100 (2016) 927–937.
[38] S. Gong, P. Cheng, Two-dimensional mesoscale simulations of saturated pool boiling from rough surfaces. Part II: bubble interactions above multi-cavities, Int. J. Heat Mass Tran. 100 (2016) 938–948.